NOAA-20 VIIRS initial on-orbit radiometric calibration using scheduled lunar observations

Taeyoung Choi[1,3*], Xi Shao[2,3], Slawomir Blonski[1,3], Wenhui Wang[1,3], Sirish Uprety[2,3], Changyong Cao[3]

[1] Global Science & Technology (GST), Inc., 7855 Walker Dr., Suite 200, Greenbelt, MD 20770, U.S.A.
[2] University of Maryland, College Park, MD 20740, U.S.A.
[3] NOAA Center for Satellite Applications and Research (STAR), 5830 University Research Ct., College Park, MD 20740-3818, U.S.A.

ABSTRACT

The scheduled lunar observations by the NOAA-20 VIIRS provide an independent source of calibration for the Reflective Solar Bands (RSB). Spacecraft roll maneuver is typically conducted to ensure that the moon observation is recorded at the Space View (SV) scan angle. VIIRS Earth View sector is shifted at the time of the lunar data collection to cover the SV scan angle and ensure spectral band co-registration. The lunar observation is performed monthly at nearly the same lunar phase angle with the exception of ~3-4 months each year. This paper analyzes scheduled lunar observations data from December 2017 to May 2019. For each lunar collection, the Global Space-based Inter-Calibration System (GSICS) Implementation of ROLO (GIRO) model is used to predict the expected lunar irradiance, and the ratio between the GIRO modeled and observed lunar irradiance is derived as the VIIRS lunar F-factor (or inverse of the gain factor). The lunar F-factors are compared to the Solar Diffuser (SD) based F-factors that are used in the operational production of VIIRS Sensor Data Records (SDR) at NOAA. These two on-orbit calibration methods provide independent trending of the radiometric response degradations in the RSBs of VIIRS. In this paper, we present SD and lunar F-factor comparison results for NOAA-20 VIIRS RSBs.

Keywords: NOAA-20, VIIRS, RSB, Solar Diffuser, SD, SDSM, Lunar, GIRO

1. INTRODUCTION

On November 18th, 2017, the second Visible Infrared Imaging Radiometer Suite (VIIRS) instrument was launched onboard the NOAA-20/JPSS-1 satellite to support Earth system monitoring and weather applications. NOAA-20 satellite operates on the same orbit as the Suomi National Polar-orbiting Partnership (S-NPP) satellite launched in 2011, the afternoon sun-synchronous orbit with the 1:30 p.m. equator crossing local time on the ascending part of the orbit. The satellites are positioned on the opposite sides of the orbit to increase frequency of the combined global observations. Same as the S-NPP VIIRS, the NOAA-20 VIIRS also provides a daily observations of the entire Earth from a nominal altitude of 824km [1-3]. VIIRS has 22 spectral bands covering 0.41μm to 12.5μm with spatial resolution of 750 and 375 meters for the Moderate-resolution (M) and Imaging (I) bands, respectively. Table 1 provides detailed information for the 22 VIIRS spectral bands. From the global observations with the 22 spectral bands, more than 26 Environmental Data Records (EDRs) are produced such as sea surface temperature, clouds, aerosol, vegetation fraction, fire, snow, polar winds, etc. Detailed documentation of the EDRs can be found at https://www.star.nesdis.noaa.gov/jpss/JPSS_products.php.

To validate VIIRS functionality and to achieve accurate SDR and EDR production, Post-Launch Tests (PLTs) were performed supported by a team of experts from several organizations and agencies including NOAA, NASA, University of Wisconsin, University of Maryland, and the Aerospace Corp. Based on the lessons learned from the Suomi NPP VIIRS

* Primary author: taeyoung.choi@noaa.gov; phone 1-301-683-3562; STAR / NESDIS / NOAA contract with GST

Earth Observing Systems XXIV, edited by James J. Butler, Xiaoxiong (Jack) Xiong, Xingfa Gu, Proc. of SPIE Vol. 11127, 111271Z · © 2019 SPIE · CCC code: 0277-786X/19/$18 · doi: 10.1117/12.2528459

cases [1], the NOAA-20 PLTs were planned and performed as listed in Cao's paper [2]. For the Reflective Solar Bands (RSBs) calibration, one of the most important PLTs was a series of yaw maneuvers that enabled measurements necessary to update the Solar Diffuser (SD) and Solar Diffuser Stability Monitor (SDSM) related LUTs and to resolve the abnormal H-factor oscillation problem [4]. In addition to the yaw maneuver data, the regular on-orbit SDSM data sets were included between the coarse yaw maneuver sampling points in the solar azimuth, especially for the SDSM Sun view attenuation screen transmittance function. The SDSM screen transmittance function derived from the combined yaw maneuver and regular on-orbit SDSM data set provided reasonable estimates of the SD degradation (H-factor) without the abnormal oscillation problems that enabled derivation of the calibration coefficients called F-factors.

Table 1. VIIRS Center Wavelength (CW), spatial resolution, gain states and typical radiance or temperature [5].

Band Name	CW [μm]	Nominal Resolution	Gain States	Ltyp or Ttyp
M1	0.412	750m	High/Low	115/44.9
M2	0.445	750m	High/Low	146/40
M3	0.488	750m	High/Low	123/32
M4	0.555	750m	High/Low	90/21
I1	0.640	375m	Single	22
M5	0.672	750m	High/Low	68/10
M6	0.746	750m	Single	9.6
I2	0.865	375m	Single	25
M7	0.865	750m	High/Low	33.4/6.4
DNB	0.7	750m	High/Mid/Low	-
M8	1.24	750m	Single	5.4
M9	1.378	750m	Single	6
I3	1.61	375m	Single	7.3
M10	1.61	750m	Single	7.3
M11	2.25	750m	Single	0.12
I4	3.74	375m	Single	270K
M12	3.70	750m	Single	270K
M13	4.05	750m	High/Low	380K/300K
M14	8.55	750m	Single	270K
M15	10.763	750m	Single	300K
I5	11.45	375m	Single	210K
M16	12.013	750m	Single	300K

After the initial update of the SDSM screen transmittance function, there was another update based on on-orbit SDSM data sets collected with the full operational range of solar azimuth. This paper provides a summary of the RSB calibration updates after the PLT period for accurate derivation of the H- and F-factors. To validate long-term detector gain changes, the SD based F-factors are compared to the lunar F-factors. To be able to calculate lunar F-factor, it requires 1) an accurate lunar irradiance model and 2) a periodic satellite observation of the moon. This paper also provides a comprehensive comparison of the two independent F-factors: the one derived from the National Institute of Standards and Technology (NIST) traceable calibration source called SD and another one derived from the GIRO lunar irradiance model. Similarities and discrepancies between long-term trends in the two F-factors are discussed here. Before explaining the calibration differences, the SD and lunar F-factors are briefly explained in the next section.

2. SD BASED ON-ORBIT RSB CALIBRATION

The NOAA-20 VIIRS has four On-Board Calibrators (OBCs) that are viewed by the Rotating Telescope Assembly (RTA) and Half Angle Mirror (HAM) with other optical components as shown in Figure 1. The RTA rotates anticlockwise in the figure starting from the left side in sequence of Space View (SV), Earth View (EV) port, blackbody (BB), and SD (the latter coincident with the SDSM measurements). The SD observation is used as a primary calibration source of the RSBs. One of the challenging issues of using the SD is the accurate estimation of the time-dependent SD degradation from exposure of the Spectralon™ surface to strong Ultraviolet (UV) light and high-energy particles. [6]. The SD degradation

is monitored by the SDSM that tracks the ratio between the near simultaneous measurements of the reference Sun views and the SD views within the desired solar angle range called 'sweet spot'.

As shown in Equation 1 and Figure 2, it is critical to get accurate measurements of the SDSM screen transmittance (τ_{SDSM}) and the product of the SD screen transmittance and the SD Bidirectional Reflectance Function in the direction of the SDSM SD view port ($\tau_{SDS} \cdot BRDF_{SDSM}$) under the sun illumination in the sweet spot range. The initial NOAA-20 VIIRS H-factors showed abnormal oscillation patterns up to 1% level, but it was later resolved by using the yaw-maneuver derived τ_{SDSM} updated with the regular on-orbit SDSM data sets [4]. Using the updated τ_{SDSM} and $\tau_{SDS} \cdot BRDF_{SDSM}$, the H-factors are calculated by Equation 1.

$$H(t) = \frac{dc_{SD} \cdot \tau_{SDSM}}{dc_{SUN} \cdot BRDF_{SDSM_{SD}} \cdot \tau_{SDS} \cdot \cos(\theta_{inc}) \cdot \Omega_{SDSM}} \quad \text{(Eq. 1)}$$

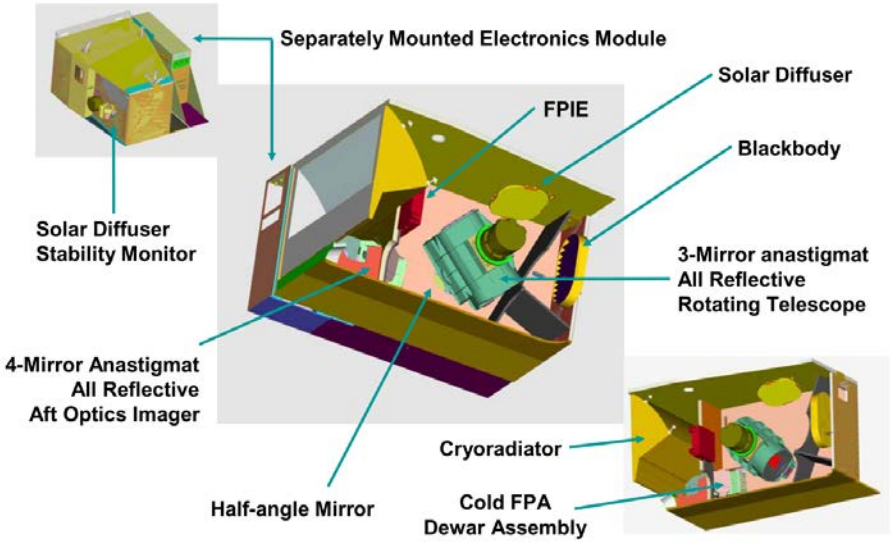

Figure 1. A 3 dimensional view of the VIIRS Opto-Mechanical Module and on-board calibrators [7].

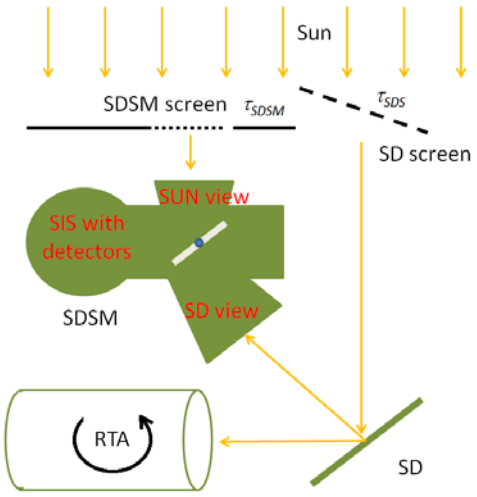

Figure 2. A relationship diagram of RTA, SD, SDSM, and SD/SDSM screens.

In the H-factor equation, dc_{SUN} is the bias removed *Digital Count (DC)* of the *Sun* view, dc_{SD} is the bias removed *DC* of the *SD* view, τ_{SDS} is the SD screen transmittance function, τ_{SDSM} is the SDSM screen transmittance, $BRDF_{SDSM\_SD}$ is the *BRDF* of the SD panel at the SDSM viewing angle, and Ω_{SDSM} is the solid angle of the SD view. Sun angle of incidence on SD is denoted by θ_{inc}.

Once the reasonable H-factors are found, the F-factors can be calculated as described in Equation 2.1 and 2.2.

$$F = \frac{\mathrm{RVS}_{SD}\cdot\cos(\theta_{inc})\cdot\{E_{sun}\cdot\tau_{sds}\cdot BRDF_{SD}\}}{C_0+C_1\cdot dn_{SD}+C_2\cdot dn_{SD}^2+C_3\cdot dn_{SD}^3} \tag{2.1}$$

$$BRDF_{SD}(t) = \frac{H(t)}{H(t_0)}\cdot BRDF_{PRE_{SD}} \tag{2.2}$$

The F-factors are calculated within the 'sweet spot' range which is defined by the solar azimuth angles from 13.60 to 30.78 degrees and solar declination angles from 14.00 to 18.39 degrees [7]. Note that the prelaunch version of SD BRDF is modified by the on-orbit H-factors at the time of the SD observations.

In Equations 2.1 and 2.2, RVS_{SD} is a Response Versus Scan angle correction factor during the SD observation, E_{sun} is the spectral band modulated solar irradiance corrected for the Sun-Earth distance, $BRDF_{SD}$ is the SD BRDF in the RTA direction, c_0, c_1, c_2 are coefficients corrected for detector and electronics temperature, and dn_{SD} is the SD digital number bias corrected from the SV response.

3. MOON BASED ON-ORBIT RSB CALIBRATION

Lunar calibration starts with a prediction of opportunities for lunar collections with roll maneuvers. With the planned roll maneuvers, VIIRS has unique chances to observe the moon through the SV port for the desired lunar phase angle of 51 degrees with waxing lunar phase. The monthly prediction procedures are described in detail by Wilson [8]. Once the scheduled lunar collection is performed, the corresponding Raw Data Records (RDRs) are processed to verified RDR (vRDR) that enables extracting the moon image as shown in Figure 3.

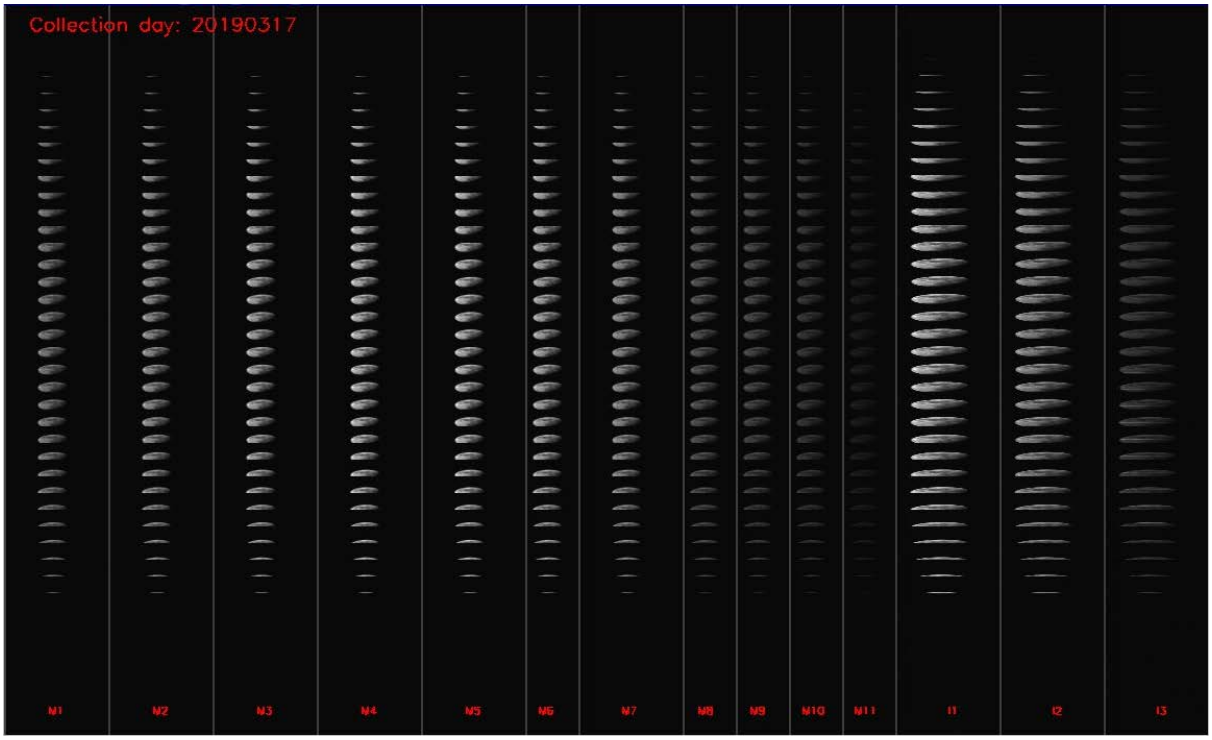

Figure 3. NOAA-20 VIIRS scheduled lunar collection image in the RSBs on March 17, 2019.

The location of SV is at the RTA scan angle of approximately -66 degrees relative to the EV nadir point as shown in Figure 1, more than 10 degrees from the edge of the EV scan. Since the NOAA-20 VIIRS is at the nominal altitude of 829 km in the ascending node, the 48 frames of SV data view approximately 3 degree beyond the Earth limb [9]. During the scheduled moon collections, VIIRS is forced to be in the high gain mode for a proper observation of the moon. Along with the fixed gain mode, EV scan sector rotation is applied to locate the center of SV at the desired EV frame. For S-NPP, the sector rotation places the moon image near the EV center frame in the 3-sample aggregation zone [10], whereas for NOAA-20, the moon image is in the no-aggregation zone just few degrees from the edge of scan.

The scheduled lunar collections can be used to measure the Band-to-Band Registration (BBR) from the selected middle scans. The BBR results suggested that the NOAA-20 VIIRS BBR have remained stable within ±0.2-pixel range in the scan direction and within ±0.05-pixel range in the track direction [11].

The U. S. Geological Survey (USGS) RObotic Lunar Observatory (ROLO) program uses the moon as an on-orbit radiometric calibration source for the remotely sensed instruments in the RSB range (https://www.moon-cal.org/main_overview.php). ROLO provides lunar irradiances at the time of satellite observation of the moon [12]. The ROLO irradiance model was derived using more than 1000 ground-based lunar observations covering a wavelength range from 0.35 to 2.45 μm with the average residual of less than 1% at each wavelength. Under the lead of European Organization for the Exploitation of Meteorological Satellites (EUMETSAT), the Global Space-based Inter-Calibration System (GSICS) international agencies and communities developed GSICS Implementation of ROLO (GIRO) lunar irradiance model with specified input and output formats [10, 13, 14].

Once the lunar irradiances are derived by the GIRO model at the time of observation, bias removed VIIRS detector responses are calculated at each band, detector, Half Angle Mirror (HAM) side, and scan, as shown in Equation 3.1. Note that the detector bias corrected Digital Numbers (DNs) are shown as lower-case 'dn' after the bias correction. The letters b, d, h, and s respectively represent VIIRS band, detector, HAM side, and scan. The bias levels are estimated from the deep space responses on either sides of the moon using 100 frames, since the OBC SV responses are not useful and valid because of the sector rotation.

$$\mathrm{dn(b,d,h,s)} = DN_{moon}(b,d,h,s) - \overline{DN_{Space}(b,d,h)} \tag{3.1}$$

Before converting to irradiance, the radiance of the lunar pixels need to be derived by applying the *c*-coefficients as shown Equation 3.2.

$$L_{pixel}(b,d,f,s) = F(b,d,h,t)_{SD} \cdot \left\{ \begin{matrix} c_0(b,d,h,s) + c_1(b,d,h,s)\cdot dn(b,d,h,s) + \\ c_2(b,d,h,s)\cdot dn(b,d,h,s)^2 + c_3(b,d,h,s)\cdot dn(b,d,h,s)^3 \end{matrix} \right\} / RVS_{SV}(b,d) \quad (3.2)$$

Please note that the polynomial goes up to the 3rd order for NOAA-20 VIIRS SWIR band radiance calculations. The 't' in the Equation 3.2 indicates the initial time of lunar collection and SD based F-factor is needed to get the lunar radiance. Even though Equation 3.2 shows c_0 coefficients, they are all set to be zero in RSB band calibration. Once the lunar radiance is calculated, the observed lunar irradiance and lunar F-factors can be derived by Equation 3.3 with the solid angle and phase angle effect.

$$F_{lunar}(b) = \frac{I_{GIRO}(b)}{I_{OBS}(b)} = \frac{I_{GIRO}(b)}{\frac{\pi \cdot R_{moon}^2}{D_{Sat\_Moon}^2} \cdot \frac{1+\cos(\vartheta)}{2} \cdot \sum_{Pixel} \frac{L_{Pixel}(b)}{N}} \tag{3.3}$$

The lunar F-factor is an irradiance based ratio as shown in Equation 3.3 since the GIRO lunar model produces lunar irradiance value. The observed lunar irradiance, I_{OBS}, can be calculated by converting accumulated lunar radiance and solid

angle calculation parts using area of the lunar disk and the distance between the satellite and moon. The actual effective area of the moon can be derived by the lunar phase angle (θ) in Equation 3.3.

4. RESULTS

NOAA-20 VIIRS Scheduled Lunar Collection

As of May 7, 2019, there have been 13 scheduled lunar collections since launch. Table 2 shows dates, UTC times, and lunar phase angles of these collections. Please note that the negative phase angles indicate the waxing lunar phases. For the NOAA-20 VIIRS scheduled lunar collections, the moon image is in the no-aggregation zone of the EV scan, except for the first collection on December 29, 2017, when the center of the moon was located in the 2-sample aggregation zone. In addition to the moon location difference, the SWIR and thermal band responses were not available during that collection because the cryo-radiator was not yet activated. As can be noticed from Table 2, the lunar phase angles are intentionally selected around a constant value (-51 degrees) to reduce possible uncertainties from the GIRO irradiance model.

Table 2. Scheduled lunar collection for NOAA-20 VIIRS.

Date	Time [UTC]	Lunar phase angle
2017-12-29*	10:03:56	-50.58
2018-1-27	19:22:49	-51.34
2018-2-26	04:47:03	-51.13
2018-3-27	12:32:59	-51.16
2018-4-25	20:21:36	-50.98
2018-5-25	05:53:34	-50.31
2018-6-23#	13:43:07	-51.42
2018-11-19	01:54:45	-50.99
2018-12-18	17:56:39	-51.32
2019-1-17	09:59:05	-50.81
2019-2-15	22:44:41	-50.84
2019-3-17#	08:11:05	-51.19
2019-4-15	15:59:10	-51.02

*Moon center was located in the 2-sample aggregation zone.

#No lunar roll maneuver was performed.

Solar Diffuser and Lunar F-factors Comparisons in the VISNIR bands

To be able to compare the long-term trends in the SD and lunar F-factors, the lunar F-factors are properly normalized to the SD F-factors in each band. Theoretically, the SD and lunar F-factors should start from unity but in reality there are some differences. The GIRO (or ROLO) lunar irradiance model was based on the Wehrli solar irradiance model with the atmospheric correction [15]. The RSB radiometric calibration of VIIRS was performed and validated using NIST traceable 100 cm Spherical Integrated Source (SIS-100). Figure 4 shows the band averaged SD F-factors in solid line with the lunar F-factors in symbols normalized by the 2nd collection point.

Please note that there is a large gap in lunar collections around 300 days since launch during the summer because the moon goes below the Earth limb. For the VIIRS bands below 1 μm, the SD and Lunar F-factors are showing very similar trends after one and half years of operation. To check these similarities and difference in the same scale, Figure 5 shows the normalized SD F-factors along with the lunar F-factors. The lunar and SD F-factors are consistently within one percent from each other, but the lunar F-factors show larger annual oscillation patterns compared to the SD F-factors in bands M1-M7, I1 and I2. Although there are annual oscillation patterns, the SD F-factors have been linearly decreasing more for the shorter wavelength bands M1 to M4. The black solid line (band M1) shows the largest decrease which would suggest that the M1 detector gains are increasing. When annual lunar F-factors are compared, it is hard to determine whether the lunar F-factors are going down like the SD F-factors because of the large annual oscillations of up to 1%. The March 17, 2019

lunar F-factors (the second symbol from the last) show larger uncertainties because there was no lunar roll maneuver and the location of moon was closer to the Earth limb than during collections with the roll maneuvers.

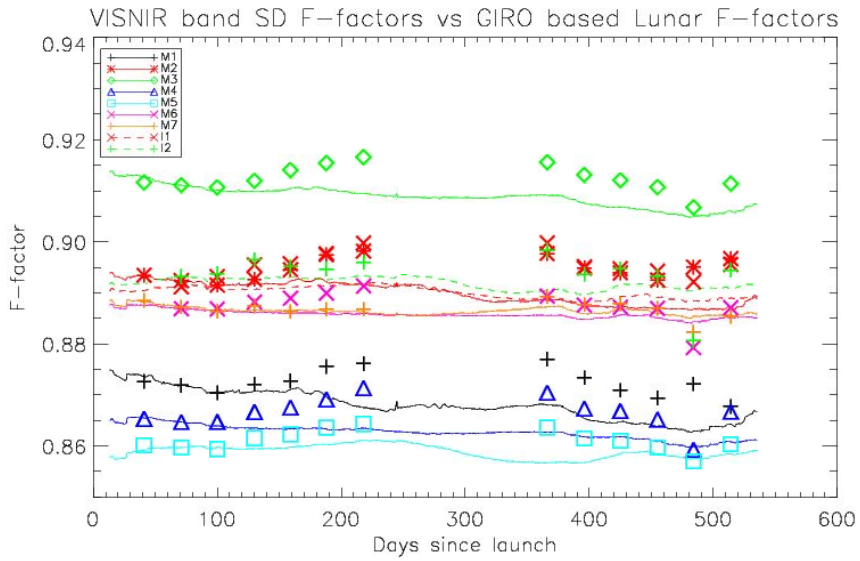

Figure 4. SD and normalized lunar F-factors for bands M1-M7, I2 and I2.

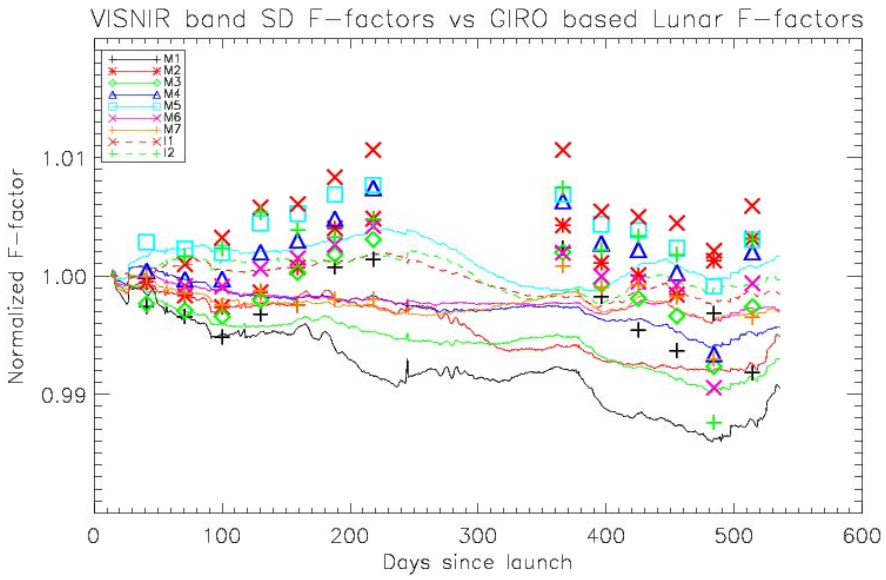

Figure 5. Normalized SD and lunar F-factors for bands M1-M7, I2 and I2.

Figure 6 shows the SWIR band comparison results with the F-factors only available after the 2nd scheduled lunar collection on January 27, 2018. Before cooling down of the cold FPA to the operational temperature with the cryoradiator door opening on January 3, 2018, SWIR band data sets were not available because of the high noise in the data. Please note that the band I3 detector 29 responses were excluded for SD and lunar F-factors since that detector was classified as non-operational (noisy) in prelaunch analyses.

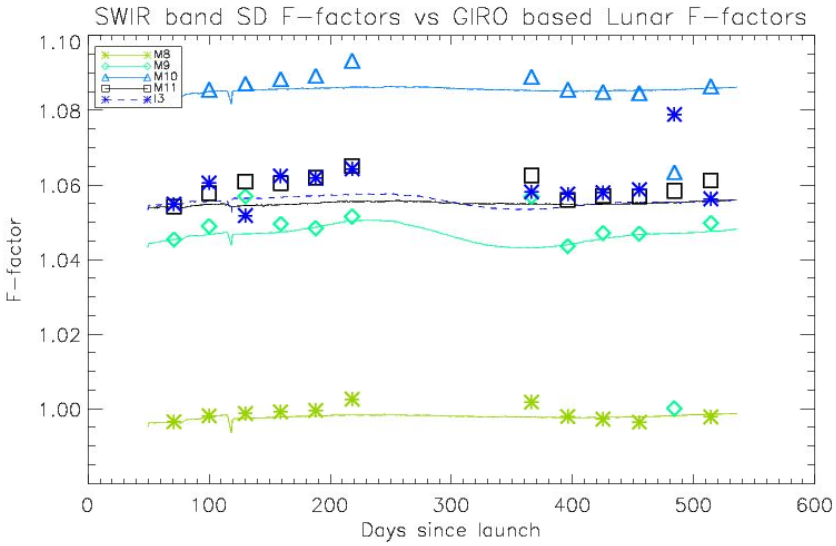

Figure 6. SD and normalized lunar F-factors for bands M8-M11 and I3.

In the SWIR bands, the SD and lunar F-factors are also showing very similar trends except the March 17, 2019 collection (the 2nd from the last symbol). In the normalized SD F-factor plot in Figure 7, there are higher variabilities in some lunar collections than in the VisNIR case shown in Figure 5, but the overall trends are very similar between the SD and lunar F-factors. With the third collection in Figure 6 and 7, the lunar F-factors became unstable because of the outgassing event on March 14, 2018. The mid-mission outgassing was conducted to remove icing in the cold FPA dewar [2].

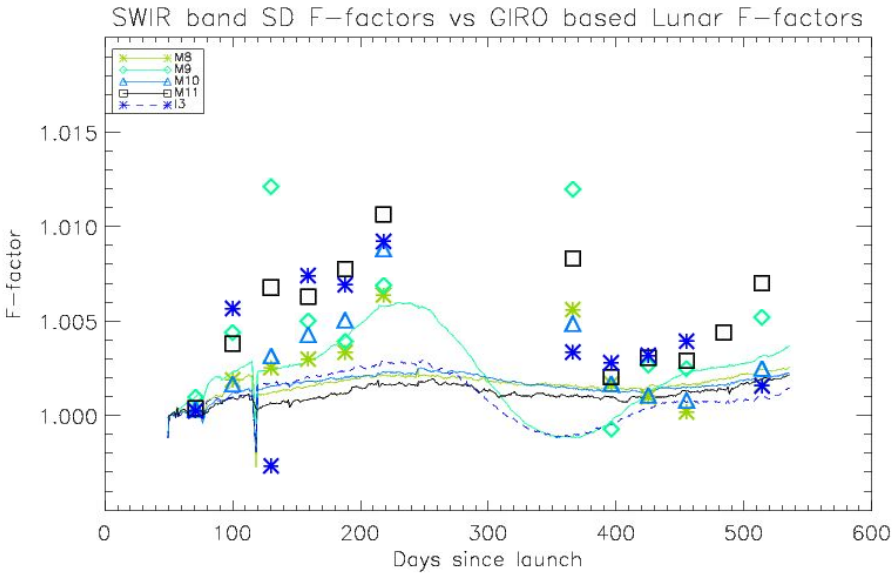

Figure 7. Normalized SD and lunar F-factors in M8~M11 and I3.

NOAA Operational F-factor

Figure 8 shows band averaged current NOAA operational F-factors that were delivered to VIIRS SDR production system called Interface Data Processing Segment (IDPS). The operational F-factors delivered in April 2018 do not have any time

dependency. Our long-term radiometric response degradation trend monitoring using cross-calibration over the pseudo-invariant desert sites and Deep Convective Cloud (DCC) observations do not show yet any evidence to support adding slopes in the operational F-factors [16]. An example of band M1 daily DCC time series is shown in Figure 9. The NOAA Calibration Center (NCC) website provides near real-time monitoring of DCC and calibration sites at https://ncc.nesdis.noaa.gov/NOAA-20/VSTS.php. Nevertheless, all of the possible calibration sources such as SD F-factors, lunar F-factors, long-term DCC trends and cross-calibration results are being monitored by the NOAA VIIRS SDR team to provide the NOAA-20 VIIRS SDR products with the best quality.

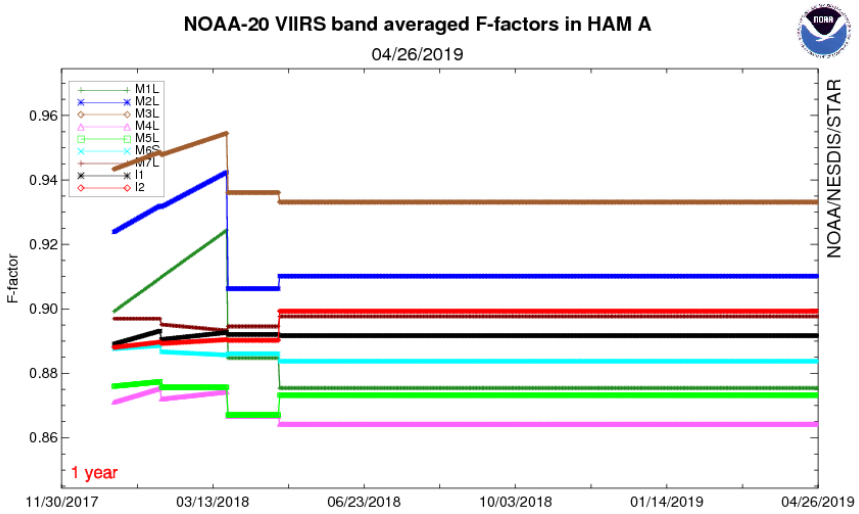

Figure 8. NOAA-20 VIIRS operational F-factor LUTs from the ICVS webpage at https://www.star.nesdis.noaa.gov/icvs/status_N20_VIIRS.php.

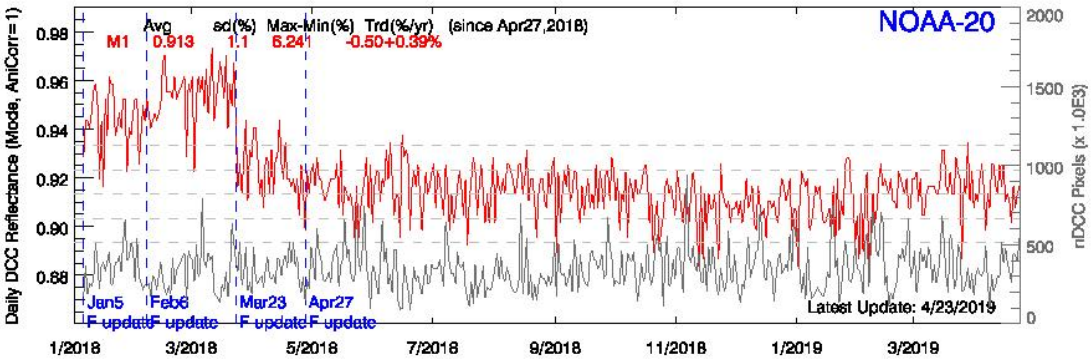

Figure 9. NOAA-20 VIIRS long-term DCC trend in band M1.

5. SUMMARY

Over one and half years of NOAA-20 VIIRS operation, the scheduled lunar collections have routinely provided independent validation for the primary SD-based VIIRS RSB radiometric calibration. NOAA VIIRS team developed and implemented an irradiance based lunar F-factor algorithm by using a lunar irradiance model called GIRO, which was developed by EUMETSAT along with the multiple international agencies such as USGS, NASA, JAXA, etc. There were 13 scheduled lunar collections as of May 8, 2019, and the corresponding lunar F-factors were calculated and compared with the SD F-factors.

Even though the lunar F-factors have shown annual oscillation patterns, the normalized SD and lunar F-factors had very similar trends (within ±1%) for all RSBs. Although both SD and lunar F-factors have so far shown decreasing patterns, especially for the first four short wavelength bands (M1-M4), no RSB radiometric calibration correction is deemed necessary since April 2018. DCC time series and results of cross-calibration with other sensors have indicated that there are no significant changes in the radiometric response. Because of the stable responses of the NOAA-20 VIIRS RSBs, the operational F-factor LUT delivered in April 2018 still remains deployed in the NOAA-20 VIIRS SDR operational processing . NOAA VIIRS SDR team is currently closely monitoring the primary SD F-factors, the secondary lunar F-factors, and long-term DCC and cross-calibration results for the best quality of the VIIRS SDR product.

Acknowledgments

Authors thank EUMETSAT for sharing the GIRO V1.0 with NOAA VIIRS team. The manuscript contents are solely the opinions of the authors and do not constitute a statement of policy, decision, or position on behalf of NOAA or the U.S. government. This work is funded by the NOAA Joint Polar Satellite System (JPSS) program.

REFERENCES

[1] C. Cao, F. J. De Luccia, X. Xiong, R. Wolfe, and F. Weng, "Early On-Orbit Performance of the Visible Infrared Imaging Radiometer Suite Onboard the Suomi National Polar-Orbiting Partnership (S-NPP) Satellite," *IEEE Transactions on Geoscience and Remote Sensing*, vol. 52, no. 2, pp. 1142-1156, 2014.

[2] C. Cao *et al.*, "NOAA-20 VIIRS on-orbit performance, data quality, and operational Cal/Val support," in *SPIE Asia-Pacific Remote Sensing*, 2018, vol. 10781, p. 9: SPIE.

[3] C. Cao *et al.*, "Suomi NPP VIIRS sensor data record verification, validation, and long-term performance monitoring," *Journal of Geophysical Research: Atmospheres*, vol. 118, no. 20, pp. 11,664-11,678, 2013.

[4] T. Choi, S. Blonski, X. Shao, and C. Cao, "Improving NOAA 20 VIIRS screen transmittance and solar diffuser BRF estimation from both Yaw maneuver and regular on-orbit data," in *SPIE Remote Sensing*, 2018, vol. 10785, p. 15: SPIE.

[5] C. Cao *et al.*, "NOAA Technical Report NESDIS 142 Visible Infrared Imaging Radiometer Suite (VIIRS) Sensor Data Record (SDR) User ' s Guide," Sep. 10, 2013 2013.

[6] X. Shao, C. Cao, and T.-C. Liu, "Spectral Dependent Degradation of the Solar Diffuser on Suomi-NPP VIIRS Due to Surface Roughness-Induced Rayleigh Scattering," *Remote Sensing*, vol. 8, no. 3, 2016.

[7] N. Baker and H. Kilcoyne, "Joint Polar Satellite System (JPSS) VIIRS Radiometric Calibration Algorithm Theoretical Basis Document (ATBD)," J. P. S. S. J. G. Project, Ed., ed. NOAA and NASA: NOAA & NASA, 2011.

[8] T. Wilson and X. Xiong, "Scheduling observations of celestial objects for Earth observing sensor calibration," in *SPIE Remote Sensing*, 2016, vol. 10000: SPIE.

[9] F. S. Patt, J. J. Butler, R. E. Eplee, R. A. Barnes, G. Meister, and J. J. Butler, "Use of the moon as a calibration reference for NPP VIIRS," presented at the Earth Observing Systems X, 2005.

[10] T. Choi, X. Shao, C. Cao, and F. Weng, "Radiometric Stability Monitoring of the Suomi NPP Visible Infrared Imaging Radiometer Suite (VIIRS) Reflective Solar Bands Using the Moon," *Remote Sensing*, vol. 8, no. 1, 2015.

[11] T. Choi, X. Shao, and C. Cao, "NOAA-20 VISIBLE INFRARED IMAGING RADIOMETER SUITE (VIIRS) ON-ORBIT BAND-TO-BAND REGISTRATION ESTIMATION FOR REFLECTIVE SOLAR BAND (RSB) USING SCHEDULED LUNAR COLLECTIONS," presented at the IGARSS, Yokohama, Japan, 2019.
[12] H. H. kieffer and T. Stone, "The Spectral Irradiance of the Moon," *The Astronomical Journal,* vol. 129, no. 6, pp. 2887-2901, 2005.
[13] T. Choi, X. Shao, and C. Cao, "On-orbit radiometric calibration of Suomi NPP VIIRS reflective solar bands using the Moon and solar diffuser," *Appl Opt,* vol. 57, no. 32, pp. 9533-9542, Nov 10 2018.
[14] T. Choi, C. Cao, and F. Weng, "RADIOMETRIC STABILITY MONITORING OF THE S-NPP VIIRS OCEAN COLOR BANDS USING THE MOON," presented at the International Symposium on Remote Sensing (ISRS), Jeju, Korea, April 20, 2016.
[15] T. Stone and H. H. Kieffer, "Absolute irradiance of the moon for on-orbit calibration," presented at the Proceedings of SPIE - The International Society for Optical Engineering, Seattle, WA, 2002.
[16] W. Wang and C. Cao, "NOAA-20 VIIRS SENSOR DATA RECORDS GEOMETRIC AND RADIOMETRIC CALIBRATION PERFORMANCE ONE YEAR IN-ORBIT," presented at the IGARSS, Yokohama Japan, 2019.